Research Square

Preprints are preliminary reports that have not undergone peer review. They should not be considered conclusive, used to inform clinical practice, or referenced by the media as validated information.

Superior and ultrafast energy storage performance of relaxor-antiferroelectric HfO2-based supercapacitors

Wentao Shuai
South China Normal University
Jiyan Dai
Hong Kong Polytechnic University https://orcid.org/0000-0002-7720-8032
Zihao Xu
South China Normal University
Guo Tian
South China Normal University
Chunlai Luo
South China Normal University
Ming Li
South China Normal University
Ruiqiang Tao
South China Normal University https://orcid.org/0000-0002-4096-3966
Zhen Fan
South China Normal University https://orcid.org/0000-0002-1756-641X
Deyang Chen
South China Normal University https://orcid.org/0000-0002-8370-6409
Guofu Zhou
South China Normal University
Xubing Lu (luxubing@m.scnu.edu.cn)
South China Normal University https://orcid.org/0000-0002-2552-9571
Jun-Ming Liu
Nanjing University https://orcid.org/0000-0001-8988-8429

Article

Keywords:

Posted Date: January 16th, 2023

DOI: https://doi.org/10.21203/rs.3.rs-2475739/v1

License: This work is licensed under a Creative Commons Attribution 4.0 International License.
Read Full License

Additional Declarations: There is **NO** Competing Interest.

Superior and ultrafast energy storage performance of relaxor-antiferroelectric HfO_2-based supercapacitors

Wentao Shuai[1], Jiyan Dai[2*], Zihao Xu[1], Guo Tian[1], Chunlai Luo[1], Ming Li[1], Ruiqiang Tao[1], Zhen Fan[1], Deyang Chen[1], Guofu Zhou[3], Xubing Lu[1*], Junming Liu[1,4]

[1] Institute for Advanced Materials and Guangdong Provincial Key Laboratory of Optical Information Materials, South China Academy of Advanced Optoelectronics, South China Normal University, Guangzhou, 510006, China

[2] Department of Applied Physics, The Hong Kong Polytechnic University, Hong Kong, P. R. China

[3] Institute of Electronic Paper Displays and Guangdong Provincial Key Laboratory of Optical Information Materials, South China Academy of Advanced Optoelectronics, South China Normal University, Guangzhou, 510006, China

[4] Laboratory of Solid State Microstructures and Innovation Center of Advanced Microstructures, Nanjing University, Nanjing 210093, China

E-mail: jiyan.dai@polyu.edu.hk

E-mail: luxubing@m.scnu.edu.cn

Abstract

Compared to electrochemical energy storage, dielectric thin film-based capacitors possess the advantages of higher voltage stability and higher break-down voltage as well as lower leakage current etc. Since HfO_2 films are compatible to microelectronic process and its ferroelectricity is strategically important in memory device, the realization of their excellent energy storage comparable or better than those perovskite oxides will broaden their applications in microelectronic devices. In this work, to combine the merits of relaxor-ferroelectric and antiferroelectric, we experimentally demonstrate that a superparaelectric-like relaxor antiferroelectric behavior can be realized in the HfO_2-based thin films and corresponding recoverable energy density over 100 J cm^{-3} can be achieved at efficiency higher than 80% as well as extremely high dielectric strength > 6 MV cm^{-1}, compared to perovskite oxide materials. This is a record high energy density in all reported HfO_2-based energy storage thin films, and beyond that, we also demonstrate their superfast charging/discharging as a capacitor. Targeting at high-speed supercapacitor applications in integrated circuit, HfO_2-based dielectric may win the competition with perovskite oxides in terms of dielectric breakdown strength and charging/discharging speed etc. Our fundamental understanding of the physics behind also enriches the knowledge of materials science and dielectric physics.

Introduction

As one of the efforts to reduce CO_2 emission and consumption of fossil fuels, energy storage by dielectric materials possesses advantages of charging-and-discharging speed (at the microsecond level) and higher temperature stability as well as higher breakdown field compared to electrochemical capacitors and battery[1-4]**.** As for thin film applications, dielectric thin film-based

energy storage enables the application for flexible and miniatured electronic devices such as sensors and actuators. However, the recoverable energy densities for linear dielectric films are much lower (2-3 orders lower) than those of electrochemical capacitors. Therefore, it is highly demanded to develop new dielectric materials to increase the recoverable energy density.

Among many strategies to increase the energy storage performance of dielectric thin films, electric polarization switching induced giant enhancement of dielectric constant is the most effective approach. As can be readily anticipated, the linear dielectric has relatively low energy density because of its low dielectric constant. By contrast, a nonlinear ferroelectric material has much larger electric polarization, hence possesses much higher permittivity. However, because of the hysteresis characteristic of ferroelectric materials, the energy stored in a ferroelectric during the charging process cannot be fully released. Instead, some of the energy is converted into heat due to the internal friction of dipole moment reorientation. As illustrated in Figure S1, the recoverable energy density (W_r) of dielectric capacitors is represented by the green area, which can be calculated by the following formula:

$$W_r = \int_{P_r}^{P_{max}} EdP \ (Discharging) \tag{1}$$

where E is the applied electric field, P_r remnant polarization and P_{max} the maximum polarization under bias electric field below breakdown strength E_b. In the equation, D is dielectric displacement contributed mainly by the electric polarization for a polarized material. Within the charge and discharge loop, the area of the loop represents the energy loss W_{loss} due to the hysteretic polarization switching, and the energy efficiency $\eta = W_r/(W_r + W_{loss})$. It is apparent that, an ideal dielectric capacitor with high energy storage properties should possess large P_{max}/P_r, high E_b and small polarization switching hysteresis area[5].

Along this direction, relaxor ferroelectrics (RFE) with much narrower *P-E* loop and antiferroelectrics with zero remnant polarization (AFE) have been demonstrated to enable further enhancement of the recoverable energy density and efficiency. Beyond these progresses, more recently, by nanodomain engineering approach, superparaelectric relaxor ferroelectric thin films of complex perovskite oxides have been demonstrated to further improve the energy performance presenting 152 J cm^{-3} with markedly improved efficiency (>90% at an electric field of 3.5 MV cm^{-1})[5]. By applying the same nanodomain engineering approach, it is also reasonable to expect the existence of superparaelectric relaxor antiferroelectric and its superior energy storage properties by combining the advantages of relaxor-ferroelectric and antiferroelectric.

In this work, for the first time, we experimentally demonstrate that a superparaelectric-like relaxor antiferroelectric characteristic (Figure S2) can be achieved in HfO_2-based thin films by doping Al into the antiferroelectric $Hf_{0.5}Zr_{0.5}O_2$ (HZO). In a 15 nm-thick Al:HZO film, corresponding recoverable energy density over 100 J cm^{-3} is achieved at an efficiency higher than 80% as well as much higher dielectric strength > 6 MV cm^{-1}. This is a record high (doubled of reported HZO thin films) energy density among all reported HfO_2-based thin films for energy storage. Compared to those perovskite oxide-based thin film capacitors, HfO_2 possesses promising features of high dielectric breakdown strength as well as ultralow leakage current[6-8]. Furthermore, the low-temperature atomic layer deposition and annealing broadens its applications to flexible and wearable electronic devices.

For a well-established material in IC industry as a high-*k* gate dielectric[9, 10], the finding of ferroelectric (FE) characteristic in doped HfO_2 may bring many new applications such as non-volatile memory and negative capacitance transistor[11, 12]. The FE behavior observed within the

HZO -based thin films is due to the formation of the non-centrosymmetric $Pca2_1$ phase, which can also be induced in HfO_2 with several other dopants such as Si, Al, Ca, Y, Sr, Lu, Gd, and La[13-16]. More recently, through interfacial strain engineering, we have obtained large ferroelectricity in HZO thin films[17-19]. In contrast to FE, antiferroelectric (AFE) behavior in the HZO (with more Zr) thin films is also known, owing to the field-induced phase transition between the nonpolar tetragonal phase ($P4_2/nmc$) and polar orthorhombic phases resulting in a double hysteresis loop[20]. The AFE characteristics can also be induced in HfO_2 with a limited number of dopants (such as Al, Si, and a solid solution of HfO_2-ZrO_2) and Al- or Si-doped $Hf_{0.5}Zr_{0.5}O_2$[21, 22]. Assisted with nano-domain engineering[23], relaxor-antiferroelectric (RAFE) properties are induced in HfO_2 with a limited number of dopants such as Al- or Si-doped $Hf_{0.5}Zr_{0.5}O_2$. The origin of the RAFE behavior is attributed to the breaking of long-range order of ferroelectricity forming nano-polar regions[24]. Herein, to combine the advantages of relaxor-ferroelectric and antiferroelectric, in this work, we experimentally demonstrated that superparaelectric-like relaxor antiferroelectric characteristics can be realized in HfO_2-based thin films presenting superior recoverable energy density and efficiency as well as ultrahigh dielectric breakdown and ultrafast charging/discharging speed[25, 26].

Results

Excellent Energy-Storage Properties. A series of W/Al:HZO/W capacitors with Al molar doping percent x varying from 0 to 4.72 were fabricated. The thickness of all Al:HZO thin films was accurately controlled to be ~15 nm by means of atomic layer deposition (ALD) process at a substrate temperature of 280 °C (see Method). Charging and discharging characteristics of these capacitors are presented by their corresponding polarization behaviours (*P-E* loops), as shown in Fig. 1a and 1b, with measured voltages of ± 6.0 V at 10 kHz. Fig. 1a illustrates the FE-AFE

transition with x increasing from 0 to 1.89, and Fig. 1b demonstrates the transition from AFE state to a relaxor-type of AFE (RAFE) state with a very narrow hysteresis loop when x further increases to more than 4.13. Recoverable energy densities W_r, P_{max}/P_r and efficiencies η defined as $W_r/(W_r+W_{loss})$ of these thin films are obtained from their unipolar P–E loops (Figure S3) at fields up to E_b and the results are summarized in Fig. 1c. One can see that the recoverable energy density gradually increases as x goes up from 0 to 4.72 with a maximum W_r = 101.4 J cm^{-3} at x= 4.13. Due to the decline of P_{max}/P_r, as shown by the red line in Fig. 1c, the W_r is subsequently reduced to 85.3 J cm^{-3} at x= 4.72 (summarized in Figure S4).

Energy storage efficiency is another essential parameter to evaluate the energy storage performance of a dielectric capacitor. One can see from Fig. 1c that the efficiency gradually increases from 40 % at x= 0 to about 80 % at x= 2.95 in accompanying with the evolution of hysteresis loop from the FE state to the AFE state; while it further increases from 60 ~ 75 % to 80 ~ 85 % upon the transition toward the RAFE state with very thin hysteresis loop (from x= 3.54 to 4.72). The increased efficiency is primarily attributed to the joint effect of reduction of W_{loss} and the reduction of leakage. In contrast to the much lower W_r of 21.73 J cm^{-3} obtained in the film without Al doping, very high recoverable energy density value (~100 J cm^{-3}) and high efficiency (over 80%) are achieved in the relaxor-AFE film with x= 4.13 Al doping.

Fig. 1d illustrates the dependence of switching current (I–E sweeps) on the Al doping level. It is apparent that without Al doping, clear peaks of current corresponding to ferroelectric switching appear at its coercive field in accordance with Fig. 1a; while Al doping at x=1.89 makes the switching current peaks more diffused shifting to a higher field than that of the FE phase. The Al doping hinders the ferroelectric switching and induces a transition from ferroelectric phase to

antiferroelectric-like phase. It is apparent that, further increased Al doping makes the ferroelectric switching current more diffused and nearly disappeared; this is an indication of relaxor characteristic, manifesting the phase transition from AFE state to relaxor AFE (RAFE) state[27].

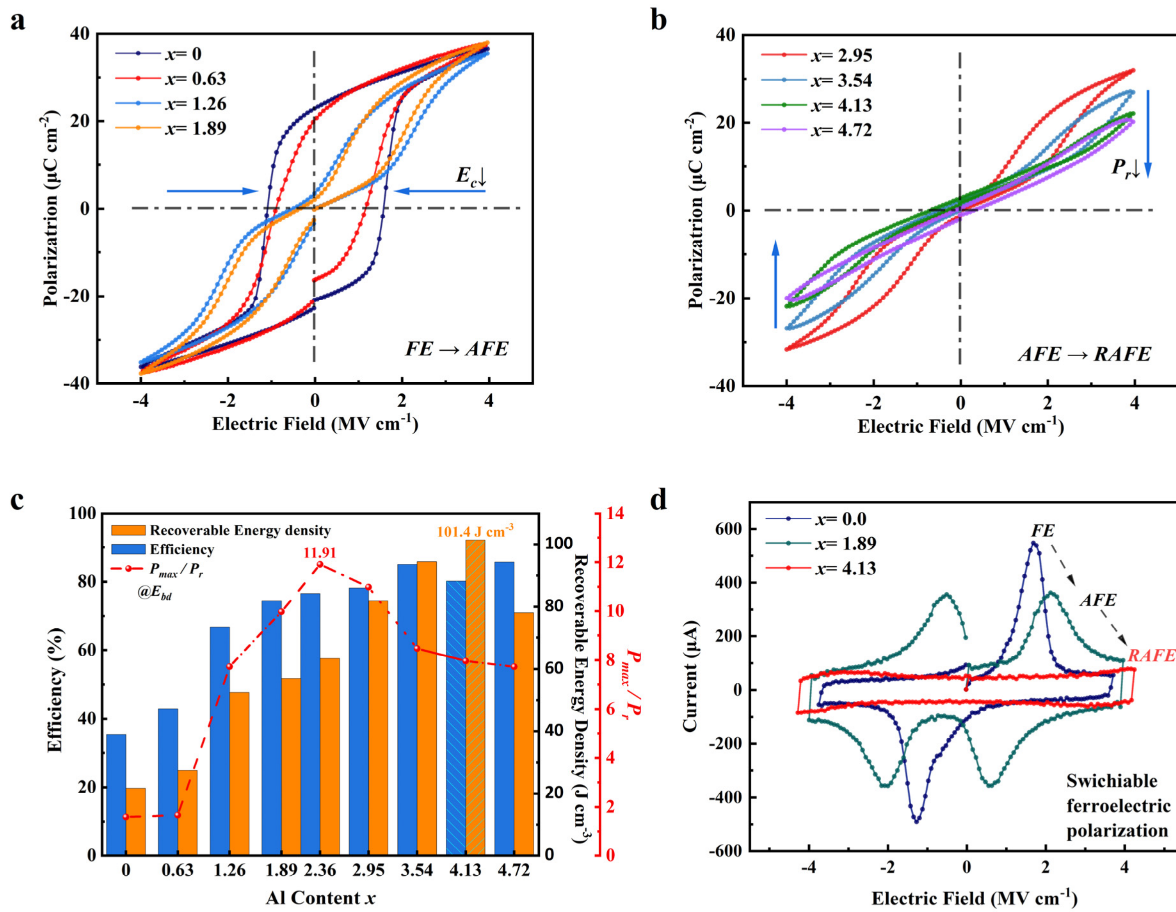

Fig. 1 | Evolution of *P-E* loops, *I–E* sweeps and energy storage performance increased Al content. a *P-E* loops from FE to AFE and **b** from AFE to RAFE at an electric field of 4 MV cm^{-1} with increasing Al content x. **c** Comparison of the energy storage performance W_r, η and P_{max}/P_r of the films with different Al content at their breakdown fields. **d** Dependence of compensation current versus electric field (*I–E*) sweeps of FE/ AFE/ RAFE Al:HZO capacitors with three different Al doping levels.

The merit of RAFE in energy storage performance is illustrated in Fig. 2a presenting a comparison of the energy densities and efficiencies of representative dielectrics from literatures. One can see that, compared to the FE and AFE materials, the relaxor AFE state significantly benefits to the enhancement of the recoverable energy density and efficiency as demonstrated in our work. As a critical parameter for energy storage application, dielectric breakdown strength of the Al:HZO films with different Al doping levels were characterized, and the results are shown in Fig. 2b (with three Al doping levels). It can be seen that, the Al-doped film with x= 4.13 not only achieves the highest W_r value, but also the highest dielectric breakdown strength > 6.0 MV cm^{-1}. This value is one of the highest among all reported oxide dielectric thin films, especially compared to those perovskite oxides with dielectric breakdown strength usually less than 1 MV cm^{-1}, and therefore is highly appreciated for energy storage application.

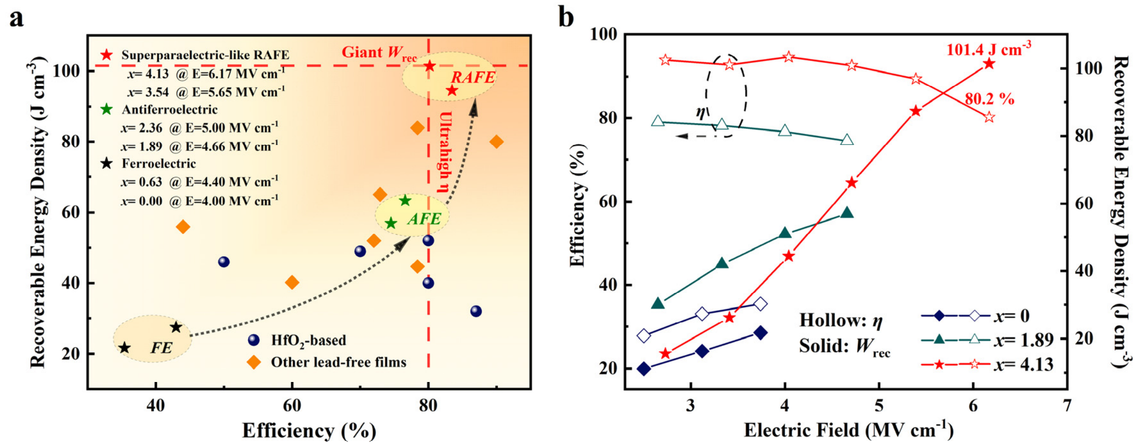

Fig. 2 | Energy storage performance of Al-doped HZO capacitors. a Comparison of energy density and efficiency of this work with representative ferroelectric thin films[8, 15, 28-36].**b** Energy density and efficiency of the of FE/ AFE/ RAFE Al:HZO capacitors as a function of electric field up to E_b.

Table 1 | Comparison of the energy storage performance of the Al:HZO films with reported HfO_2-based dielectric films.

Dielectric films	W_{rec} (J cm^{-3})	η (%)	E_{max} or E_b (MV cm^{-1})	*Ref.*
$Hf_xZr_{1-x}O_2$	46	~50	4.5	[35]
Si-HfO_2	~40	~80	~3.3	[30]
Si-HfO_2	61.2	65	4.5	[38]
Si-$Hf_{0.5}Zr_{0.5}O_2$	40-53	~80	4.75	[36]
La-$Hf_{0.5}Zr_{0.5}O_2$	49	70	~4	[15]
Al-$Hf_{0.5}Zr_{0.5}O_2$	52	80	5.0	[37]
Al_2O_3: DIL-$Hf_{0.5}Zr_{0.5}O_2$	54.3	51.3	4-5.5	[29]
FE-$Hf_{0.5}Zr_{0.5}O_2$	**21~27**	**35~43**	**4~4.4**	**This Work**
AFE-$Hf_{0.5}Zr_{0.5}O_2$	**~57**	**~75**	**~4.67**	**This Work**
RAFE-$Hf_{0.5}Zr_{0.5}O_2$	**~100**	**~80**	**~6.17**	**This Work**

In Table 1, we compare the energy storage performance of the films in this work with reported HfO_2-based dielectrics films. For example, the AFE $Hf_xZr_{1-x}O_2$ shows a W_r of 46 J cm^{-3} at 4.5 MV cm^{-1} with energy efficiency around 50% over a wide temperature range[35]. Hoffmann *et al*[30] reported a superior energy storage performance in Si doped HfO_2 (Si-HfO_2) having 9 nm thickness with a W_r ~40 J cm^{-3} and an energy efficiency of ~80% at 3.3 MV cm^{-1}. Lomenzo *et al* reported ALD deposited Al-doped $Hf_{0.5}Zr_{0.5}O_2$ thin films with AFE behavior[37], but with a not so high W_r of

52 J cm^{-3} as well as ~ 80% for η. Ali *et al*[38] have grown Si-HfO_2 (10 nm)/TiN (10 nm) stack film on silicon substrates using ALD technique; due to their AFE nature, these films have shown relatively high W_r of 61.2 J cm^{-3} with an efficiency of 65% at 4.5 MV cm^{-1}. Silva *et al* [29] reported a high energy storage performance in ZrO_2 binary oxide films by coupling it with a low permittivity HfO_2:Al_2O_3 (HAO) layer of different thickness. Through interfacial polarization, the HAO layer improved the ferroelectric and energy storage capabilities of the ZrO_2. La-doped $Hf_{0.5}Zr_{0.5}O_2$ AFE thin films with W_r of 49 J cm^{-3} and η of 70%[15] are reported as well. We conclude that, compared to reported results, our relaxor-AFE achieved more than 50% increased recoverable energy density with excellent efficiency and dielectric breakdown strength.

For practical applications, reliability for large number of cycles (high frequency stability), high voltage stability and temperature stability are essential for dielectric capacitors. In the cycling reliability test, the films were charged and discharged repeatedly at an sweeping electric field of 2.67 MV cm^{-1}, and the energy storage properties were calculated from Figure S5a-c and plotted as shown in Fig. 3a. The film with x= 4.13 can survive after 1×10^{10} cycles with almost no loss of performance. As shown in Fig. 3b, we evaluated the performance stability over a wide temperature range from -100 to 100 °C[39] , obtained by Figure S5d-f. We attribute the excellent cycling and temperature stability to Al-doping induced high dielectric breakdown strength E_b and low leakage current; both of them are highly desired for lowering the possibility of irreversible device failure. An enhanced E_b guarantees a wider range of safe-operating voltages for dielectric capacitors, and the reduction of leakage current suppresses self-discharge. The leakage current and dielectric breakdown properties of the films were measured, and the results are shown in Fig. 3c. One can see that the Al:HZO films exhibit enhanced breakdown strength E_b with increased Al content. The

characteristic E_b of the films, derived from the analysis of Weibull distribution for each component, shows a corresponding trend with respect to the resistivity (see Supplementary Method 1).

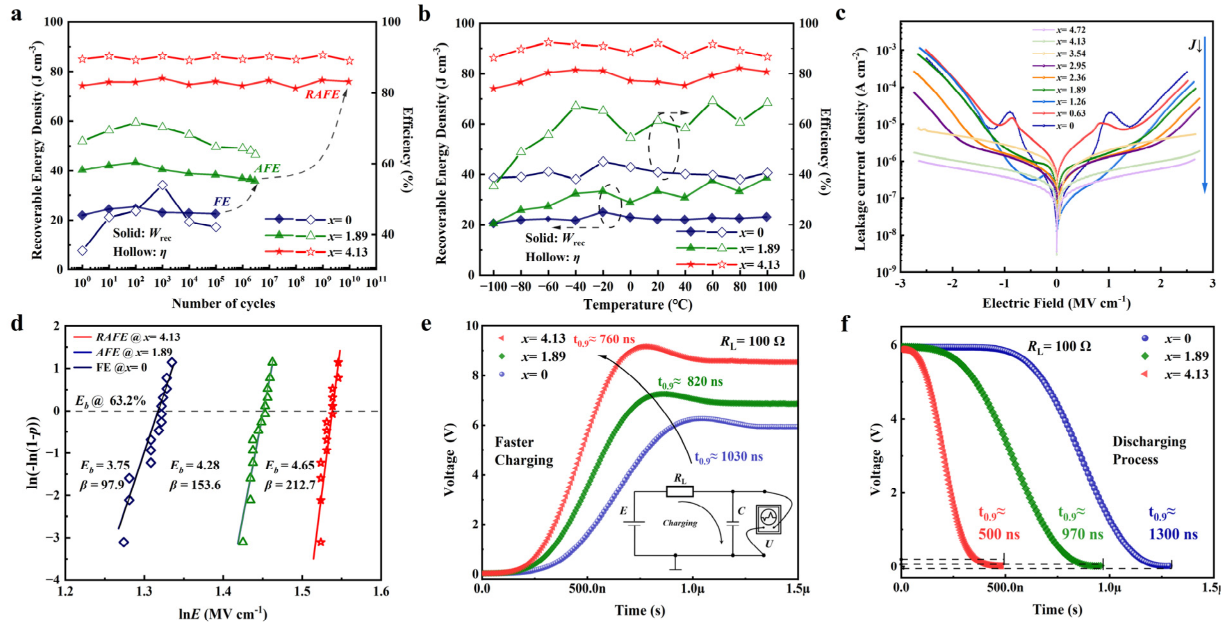

Fig. 3 | Reliability and charging/discharging tests of the Al-doped HZO films. a Charging–discharging fatigue reliability and **b** temperature-dependent energy storage properties of FE/ AFE/ RAFE Al:HZO capacitors with three different Al doping levels, with x= 0.0, x= 1.89 and x= 4.13, respectively. **c** Leakage current densities as a function of applied bias electric field. **d** Weibull distribution analysis of the breakdown fields of the films. The β is the Weibull modulus, an index of the dispersion of data distribution. E_b represents the tested breakdown field of each specimen. **e** Charging and **f** discharging voltage as functions of time for HZO film capacitors with different Al-doping ratios.

As shown in Fig. 3d, two-parameter Weibull distribution function was employed to analysis the breakdown behavior of samples. The statistical E_b values derived from the Weibull distribution analysis are 4.65 MV cm^{-1} for x= 4.13 and 4.28 MV cm^{-1} for x= 1.89, which is much higher than the film with x= 0.0 (3.75 MV cm^{-1}). Also, we found that the distribution of E_b becomes narrower as x increases, indicating the high quality of the films. The dielectric film with smaller grain sizes and higher density of domain boundaries tends to possess a higher resistivity and a larger

breakdown strength. The breakdown field strength is generally higher for ALD-deposited HfO_2 (> 6 MV cm^{-1}) compared with other ferroelectric materials, such as Pb $(Zr,Ti)O_3$ and $BaTiO_3$ whose breakdown strengths are typically lower than 1 MV cm^{-1}, enabling the HfO_2-based devices for a wider range of applications[40, 41].

The charging/discharging time of dielectric capacitors, generally described by $t_{0.9}$, refers to the time used to store or release 90% of the total energy of a capacitor which is another key parameter to determine the application potential[42] . In practice, the charging/discharging time of a capacitor is mainly determined by the RC (resistor-capacitor) delay in the circuit. Fig. 3e and 3f compare the charging and discharging speed, respectively, of the three types of HZO film capacitors, FE/ AFE/ RAFE, in a RC circuit. As can be seen from Fig. 3f, the HZO film capacitor of RAFE has the fastest charge/discharge times compared to FE and AFE. According to Supplementary Table 1, this charging/discharging performance also shows a clear superiority compared to some other reported results. We conclude that the RAFE Al:HZO film capacitors exhibit excellent charging/discharging performance and offer good prospects for high-speed pulsed power applications, etc[43, 44].

Microstructure of Superparaelectric-Like Films. To reveal the origin of the excellent energy storage properties and reliability of Al:HZO thin films from the perspective of microstructure and crystal phase transition, XRD characterization of various Al:HZO films with various concentration (x= 0~4.72) were carried out. As shown in Fig. 4a, the absence of diffraction peaks of (111) planes of m-phase HZO indicates that the formation of m-phase is suppressed. For the pure HZO film without Al doping, a distinct diffraction peak corresponding to the (111) planes of o and t-phases

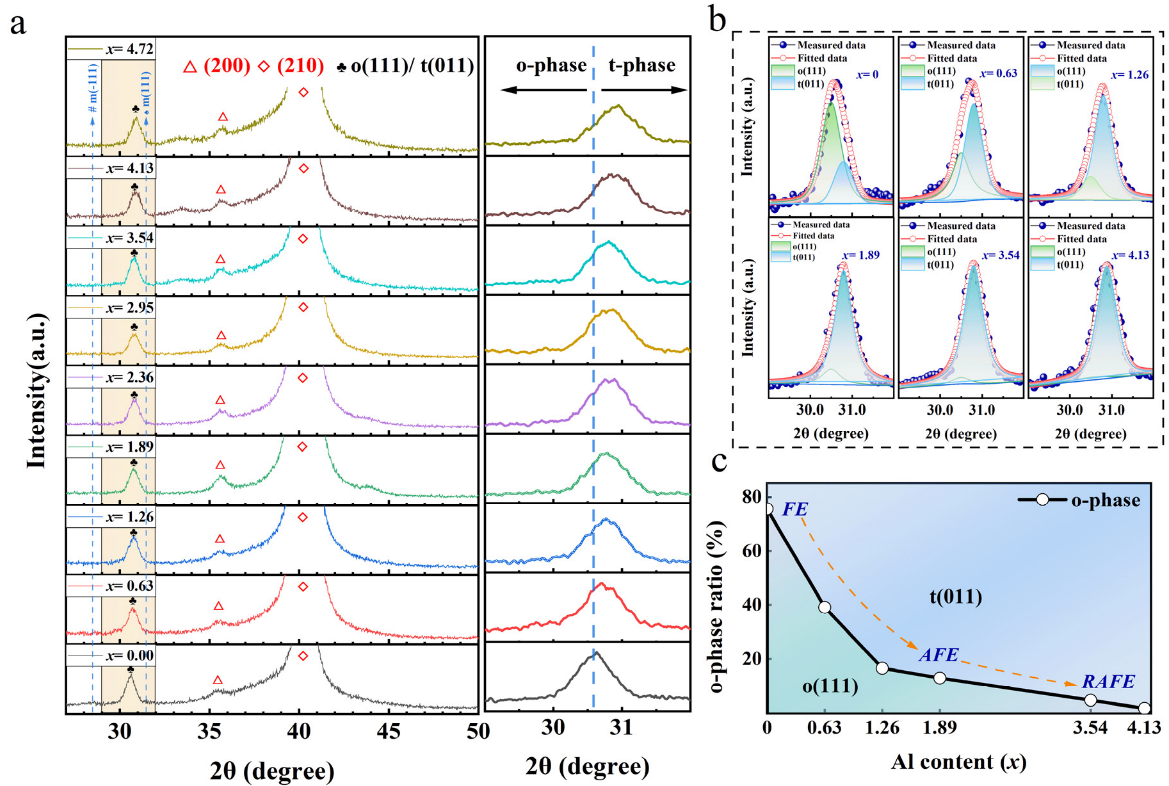

Fig. 4 | Phase evolution with increasing Al content *x*. **a** Room-temperature Grazing-incidence X-ray diffraction (GIXRD) patterns of the films. The right graph shows the fine scanning of the (111) and (011) diffraction peaks of the orthorhombic and tetragonal phases in the orange area. **b** Deconvolution of GIXRD extracted from **a** and **c** summary of the relative ratio fractions of o/t-phase in the Al:HZO thin film samples from $x= 0$ to $x= 4.13$.

can be identified; and one can also see the right shift of this diffraction peak when Al content increases. To obtain the phase fraction of o(111)/t(011), GIXRD plots of the deconvolution from $x= 0$ to $x= 4.13$ Al:HZO films representing FE, AFE, and RAFE, respectively, are shown in Fig. 4b. The relative content of each phase can be obtained by calculating the integrated area under each Gaussian peak[45]. It is apparent that the fractions of o-phase in samples $x= 0$ (75.6%), $x= 0.63$ (39.1%), $x= 1.89$ (16.7%), $x= 3.54$ (4.8%), and $x= 4.13$ (3.3%) gradually decrease with increasing Al-doping ratio (see Fig. 4c); while the proportion of t-phase changes in an opposite way. This

result indicates that the tetragonal phase becomes more stable with the increase of Al doping concentration, ensuring high E_b and low P_r[46].

We attribute the relaxor antiferroelectric characteristics to the formation of nanodomains due to the doping of AlO_x to the HZO film. By comparing the PFM images of the Al:HZO film with x= 4.13 (Fig. 5a,b) with the pure HZO film (Fig. 5d,e), one can see that, the domain size of the Al

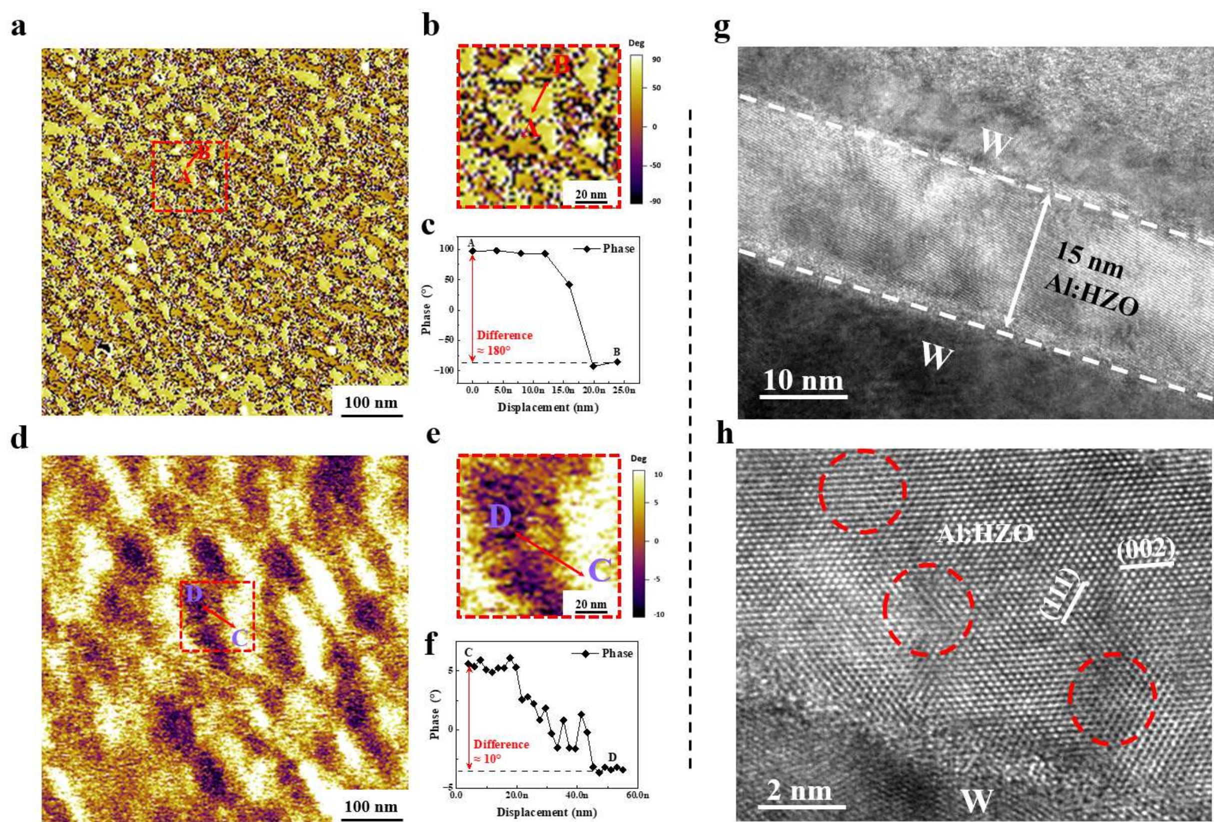

Fig. 5 | Disordered nanostructures and nanodomains in RAFE HZO film. PFM phase images of **a**, **b** the RAFE (x= 4.13), and **d**, **e** the FE pure HZO thin films with applying a DC bias write voltage (V_{dc}) of 3.0 V as well as **c, f** the corresponding phase plot**. g, h** Cross-section TEM images of x= 4.13 mol% Al-doped $Hf_{0.5}Zr_{0.5}O_2$ films.

doped film is much smaller (a few nanometers) than that of the pure HZO film which is a few tens of nanometers. It is also worthy to note that even at 3V, the x=4.13 Al:HZO film realizes

polarization switching manifested by the nearly 180° phase angle change (Fig. 5c) due to polarization switching (see the area indicated by red line); while the same voltage only induces a small phase change as shown in Fig. 5f, implying very limited polarization switching in HZO film. The different phase change behaviors further verify the existence of nanodomains in the Al:HZO (x= 4.13) samples. Al doping into the HZO film interrupts the long-range periodic structure of HZO and introduces disordered nanostructures, as can be suggested by the cross-sectional HRTEM images shown in Fig. 5g and Fig. 5h, in which the disordered structure can be clearly seen in the circled areas. This disordered structure of the Al:HZO phase contributes not only to the formation of nanodomains but also to facilitate the switching of nanodomains and reduce energy dissipation, i.e. a characteristic of relaxor ferroelectric.[23] The RAFE characteristics greatly enhance the recoverable energy density and efficiency, and the weak interactions between nanodomains may also give rise to faster charging/discharging speed of the capacitor.

Conclusion

In summary, we have demonstrated a new superparaelectric approach to realize superior energy storage performance (W_r over 100 J cm^{-3} and efficiency higher than 80%) along with ultrahigh charging/discharging speed in Al-doped relaxor antiferroelectric $Hf_{0.5}Zr_{0.5}O_2$ films. Besides superior energy storage performance, excellent fatigue properties (>10^{10} cycles with W_r over 70 J cm^{-3}) and thermal stability up to ~100 °C. Based on the advantages of ALD preparation and compatibility with standard CMOS manufacturing, it shows great advantages for integrated energy storage capacitor applications that require miniaturization and integration. These favorable features indicate that HfO_2-based superparaelectric-like dielectric thin films could exhibit a great potential for high-energy density applications in microdevices.

Methods

Fabrication of devices: The W/ Al: HZO/ W capacitors with superior energy performance were successfully prepared by ALD on Si substrate. The key process flow for the types of capacitors is illustrated below. First, metal films of W were used as bottom electrodes forming into a capacitor structure. W bottom electrodes with a thickness of 50 nm were deposited on Si wafer (100) substrates via DC reactive sputtering. Next, ~15 nm-thick Al-doped HZO films were deposited by atomic layer deposition (ALD) at a substrate temperature of 280 °C. In ALD deposition, thin film growth occurs as a sequence of precursor pulses which deposit an atomic layer of material per pulse. The ratio of Al, Hf and Zr was adjusted by changing the sequence and number of the three precursors. Meanwhile, tetrakis (dimethylamino) zirconium, tetrakis (dimethylamido) hafnium, trimethylaluminum and O_3 were used as the ALD precursors for Zr, Hf, Al and oxygen, respectively. The growth per cycle of HfO_2 and ZrO_2 were almost identical (≈Å/cycle). By means of homogeneous doping, the (Hf + Zr)/Al ALD cycle ratio varied from 37: 1 to 7: 1(0.63~4.72 mol%), which led to the incorporation of 1 to 9 cycles of Al doping, respectively. Nine different films with 0, 0.63, 1.26, 1.89, 2.36, 2.95, 3.54, 4.13, and 4.72 mol% Al-concentrations were grown. The details for calculation of the Al-concentration are presented in the Supplementary Method 1. For instance, for 18:1 ratio films, the sequence of ALD was performed with alternating pulses of Hf and Zr to a total of 18 combined pulses, then a dopant pulse would occur. The sequence was repeated to achieve a film thickness of ~15 nm. Then, the different top electrodes (50 nm for W) were sputtering deposited onto HZO films as a contact pad with 100 μm diameter. In addition, different annealing temperatures were found to be critical to the performance and were optimized. For example, we found that 300-600 ºC is a favorable temperature range for crystallization.

Therefore, in this work, all the capacitors were crystallized by rapid thermal annealing (RTA) at 550 °C in a N_2 atmosphere for 30 s.

Characterization: For electrical characterization, the ferroelectric, dielectric, and leakage current properties were measured with Radiant Precision, Agilent B1500A semiconductor product analyzer, and E4990A impedance analyzer, respectively. To avoid the Sawyer-Tower circuit being affected by reverse voltage and parasitic capacitance during the measurement, the Premier Multiferroic II ferroelectric test system from Radiant Technologies, USA, was used to measure the hysteresis loops, polarization flip current-voltage curves, and fatigue characteristics of Al: HZO ferroelectric films in this thesis work. The crystal structures of HZO film with various Al content were examined by grazing incidence X-ray diffraction (GIXRD, PANalytical X' Pert Pro diffractometer) with an incidence angle of 3.0°. The microstructures of HZO film and top/bottom interfaces were investigated by a high-resolution transmission electron microscope (HRTEM, JEM2100F) using a cross-sectional specimen. To evaluate the actual discharge performance, the charging-discharging test system in the RC circuit is built by ourselves and recorded by LeCroy Rico 64Xi-A Oscilloscope. The ferroelectric domain structures of the devices were characterized by PFM (Cypher, Asylum Research) using conductive PFM probes (Arrow EFM, Nanoworld).

Data availability

The data that support the findings of this study are available from the corresponding author upon reasonable request.

References

1. Q. Li*, et al.* Flexible high-temperature dielectric materials from polymer nanocomposites. *Nature* **536**, 112 (2016).

2. H. Palneedi, M. Peddigari, G. T. Hwang, D. Y. Jeong &J. Ryu. High-Performance Dielectric Ceramic Films for Energy Storage Capacitors: Progress and Outlook. *Adv Funct Mater* **28**, 33 (2018).

3. Q. Li, J. Chen, L. Fan, X. Kong &Y. Lu. Progress in electrolytes for rechargeable Li-based batteries and beyond. *Green Energy & Environment* **1**, 18-42 (2016).

4. N. Meng*, et al.* Ultrahigh beta-phase content poly(vinylidene fluoride) with relaxor-like ferroelectricity for high energy density capacitors. *Nat Commun* **10**, 4535 (2019).

5. H. Pan*, et al.* Ultrahigh energy storage in superparaelectric relaxor ferroelectrics. *Science* **374**, 100-104 (2021).

6. T. S. Böscke, J. Müller, D. Bräuhaus, U. Schröder &U. Böttger. Ferroelectricity in hafnium oxide thin films. *Appl Phys Lett* **99**, 102903 (2011).

7. J. Muller*, et al.* Ferroelectricity in Simple Binary ZrO_2 and HfO_2. *Nano Lett* **12**, 4318-4323 (2012).

8. S. Mueller*, et al.* Incipient Ferroelectricity in Al-Doped HfO_2 Thin Films. *Adv Funct Mater* **22**, 2412-2417 (2012).

9. J. Y. Dai, P. F. Lee, K. H. Wong, H. L. W. Chan &C. L. Choy. Epitaxial growth of yttrium-stabilized HfO_2 high-k gate dielectric thin films on Si. *J Appl Phys* **94**, 912-915 (2003).

10. P. F. Lee, J. Y. Dai, K. H. Wong, H. L. W. Chan &C. L. Choy. Growth and characterization of Hf-aluminate high-k gate dielectric ultrathin films with equivalent oxide thickness less than 10 angstrom. *J Appl Phys* **93**, 3665-3667 (2003).

11. M. A. Alam, S. Mengwei &P. D. Ye. A Critical Review of Recent Progress on Negative Capacitance Field-Effect Transistors. *Appl Phys Lett*, **114**, 090401 (2019).

12. K. C. Chan, P. F. Lee &J. Y. Dai. Study of tunneling mechanism of Au nanocrystals in HfAlO matrix as floating gate memory. *Appl Phys Lett* **92**, 223105 (2008).

13. S. S. Cheema*, et al.* Enhanced ferroelectricity in ultrathin films grown directly on silicon. *Nature* **580**, 478-482 (2020).

14. Y. Goh, J. Hwang &S. Jeon. Excellent Reliability and High-Speed Antiferroelectric $Hf_{0.5}Zr_{0.5}O_2$ Tunnel Junction by a High-Pressure Annealing Process and Built-In Bias Engineering. *ACS Appl Mater Interfaces* **12**, 57539-57546 (2020).

15. M. G. Kozodaev, *et al.* La-doped $Hf_{0.5}Zr_{0.5}O_2$ thin films for high-efficiency electrostatic supercapacitors. *Appl Phys Lett* **113**, 123902 (2018).

16. X. H. Sang, E. D. Grimley, T. Schenk, U. Schroeder &J. M. LeBeau. On the structural origins of ferroelectricity in HfO_2 thin films. *Appl Phys Lett* **106**, 162905 (2015).

17. Y. Zhang, *et al.* Enhanced Ferroelectric Properties and Insulator-Metal Transition-Induced Shift of Polarization-Voltage Hysteresis Loop in VO_x-Capped $Hf_{0.5}Zr_{0.5}O_2$ Thin Films. *ACS Appl Mater Interfaces* **12**, 40510-40517 (2020).

18. Z. M. Zou, *et al.* Enhancement of ferroelectricity and homogeneity of orthorhombic phase in $Hf_{0.5}Zr_{0.5}O_2$ thin films. *Nanotechnology* **32**, 6 (2021).

19. H. M. Yau, X. X. Chen, C. M. Wong, D. Y. Chen &J. Y. Dai. Orientation control of phase transition and ferroelectricity in Al-doped HfO_2 thin films. *Mater Charact* **176**, 111114 (2021).

20. S. W. Ryu, *et al.* Effects of ZrO_2 doping on HfO_2 resistive switching memory characteristics. *Appl Phys Lett* **105**, 072102 (2014).

21. S. W. Lee, C.-M. Kim, J.-H. Choi, C.-M. Hyun &J.-H. Ahn. Modulation of crystal structure and electrical properties of $Hf_{0.6}Zr_{0.4}O_2$ thin films by Al-doping. *Materials Letters* **252**, 56-59 (2019).

22. L. Zhao, J. R. Liu &Y. Zhao. Systematic studies of the effects of group-III dopants (La, Y, Al, and Gd) in $Hf_{0.5}Zr_{0.5}O_2$ ferroelectrics by ab initio simulations. *Appl Phys Lett* **119**, 172903 (2021).

23. H. Pan, *et al.* Ultrahigh-energy density lead-free dielectric films via polymorphic nanodomain design. *Science* **365**, 578-582 (2019).

24. R. A. Cowley, S. N. Gvasaliya, S. G. Lushnikov, B. Roessli &G. M. Rotaru. Relaxing with relaxors: a review of relaxor ferroelectrics. *Adv Phys* **60**, 229-327 (2011).

25. H. Huang &J. F. Scott. *Ferroelectric materials for energy applications*. John Wiley & Sons (2018).

26. V. V. Shvartsman, D. C. Lupascu &D. J. Green. Lead-Free Relaxor Ferroelectrics. *J AM CERAM SOC* **95**, 1-26 (2012).

27. L. E. Cross. Relaxor ferroelectrics. *Ferroelectrics* **76**, 241-267 (1987).

28. X. Hao, Y. Wang, L. Zhang, L. Zhang &S. An. Composition-dependent dielectric and energy-storage properties of (Pb,La)(Zr,Sn,Ti)O_3 antiferroelectric thick films. *Appl Phys Lett* **102**, 163903 (2013).

29. J. P. B. Silva*, et al.* Energy storage performance of ferroelectric ZrO_2 film capacitors: effect of HfO_2:Al_2O_3 dielectric insert layer. *J Mater Chem A* **8**, 14171-14177 (2020).

30. M. Hoffmann*, et al.* Ferroelectric phase transitions in nanoscale HfO_2 films enable giant pyroelectric energy conversion and highly efficient supercapacitors. *Nano Energy* **18**, 154-164 (2015).

31. Z. Liang*, et al.* Flexible lead-free oxide film capacitors with ultrahigh energy storage performances in extremely wide operating temperature. *Nano Energy* **57**, 519-527 (2019).

32. J. P. B. Silva*, et al.* High‐Performance Ferroelectric–Dielectric Multilayered Thin Films for Energy Storage Capacitors. *Adv Funct Mater* **29**, 1807196 (2018).

33. B.-z. Shen, Y. Li &X. Hao. Multifunctional All-Inorganic Flexible Capacitor for Energy Storage and Electrocaloric Refrigeration over a Broad Temperature Range Based on PLZT 9/65/35 Thick Films. *ACS Appl Mater Interfaces* **11**, 34117-34127 (2019).

34. Q. Fan*, et al.* Significantly enhanced energy storage density with superior thermal stability by optimizing $Ba(Zr_{0.15}Ti_{0.85})O_3/Ba(Zr_{0.35}Ti_{0.65})O_3$ multilayer structure. *Nano Energy* **51**, 539-545 (2018).

35. M. H. Park*, et al.* Thin $Hf_xZr_{1-x}O_2$Films: A New Lead-Free System for Electrostatic Supercapacitors with Large Energy Storage Density and Robust Thermal Stability. *Adv Energy Mater* **4**, (2014).

36. Z. X. Sun*, et al.* Ultrahigh Energy Storage Performance of Lead-Free Oxide Multilayer Film Capacitors via Interface Engineering. *Adv Mater* **29**, 6 (2017).

37. P. D. Lomenzo, C.-C. Chung, C. Zhou, J. L. Jones &T. Nishida. Doped $Hf_{0.5}Zr_{0.5}O_2$ for high efficiency integrated supercapacitors. *Appl Phys Lett* **110**, 232904 (2017).

38. F. Ali*, et al.* Silicon-doped hafnium oxide anti-ferroelectric thin films for energy storage. *J Appl Phys* **122**, 144105 (2017).

39. J. K. Liu*, et al.* A synergistic two-step optimization design enables high capacitive energy storage in lead-free $Sr_{0.7}Bi_{0.2}TiO_3$-based relaxor ferroelectric ceramics. *J Mater Chem A* **11**, 609-620 (2023).

40. A. R. Jayakrishnan*, et al.* Are lead-free relaxor ferroelectric materials the most promising candidates for energy storage capacitors? *Prog Mater Sci* **132**, 101046 (2023).

41. H. Qi, A. Xie, A. Tian &R. Zuo. Superior Energy-Storage Capacitors with Simultaneously Giant Energy Density and Efficiency Using Nanodomain Engineered $BiFeO_3$-$BaTiO_3$-$NaNbO_3$ Lead-Free Bulk Ferroelectrics. *Adv Energy Mater* **10**, 1903338 (2020).

42. F. Yan*, et al.* Significantly enhanced energy storage density and efficiency of BNT-based perovskite ceramics via A-site defect engineering. *Energy Storage Mater* **30**, 392-400 (2020).

43. C. Yang*, et al.* Fatigue-Free and Bending-Endurable Flexible Mn-Doped $Na_{0.5}Bi_{0.5}TiO_3$-$BaTiO_3$-$BiFeO_3$ Film Capacitor with an Ultrahigh Energy Storage Performance. *Adv Energy Mater* **9**, 1803949 (2019).

44. Q. L. Fan*, et al.* Realization of high energy density in an ultra-wide temperature range through engineering of ferroelectric sandwich structures. *Nano Energy* **62**, 725-733 (2019).

45. V. Gaddam, D. Das &S. Jeon. Insertion of HfO_2 Seed/Dielectric Layer to the Ferroelectric HZO Films for Heightened Remanent Polarization in MFM Capacitors. *Ieee T Electron Dev* **67**, 745-750 (2020).

46. H. Yang, H.-J. Lee, J. Jo, C. H. Kim &J. H. Lee. Role of Si Doping in Reducing Coercive Fields for Ferroelectric Switching in HfO_2. *Phys Rev Appl* **14**, 064012 (2020).

Acknowledgments

This work is supported by Hong Kong Research Grant Council (No. 15300622), National Natural Science Foundation of China (Nos. 52250281, 62174059). This work is also supported by Guangdong Science and Technology Project-International Cooperation (No. 2021A0505030064), Guangdong Provincial Key Laboratory of Optical Information Materials and Technology (No. 2017B030301007).

Author contributions

J. D. and X. L. conceived and supervised the research. W.S. prepared the devices and performed the GIXRD and electrical measurements. J. D. performed the HRTEM measurements. Z. X. and G.T. conducted the PFM measurements. W. S., J. D., X. L. and J. L. wrote and revised the manuscript. All authors discussed the results and commented on the manuscript.

Competing interests

The authors declare no competing interests.

Supplementary Files

This is a list of supplementary files associated with this preprint. Click to download.

- SupplementaryInformation.pdf